

See discussions, stats, and author profiles for this publication at: <https://www.researchgate.net/publication/372654682>

A Discontinuous Galerkin Finite Element Model for Compound Flood Simulations

Preprint · July 2023

DOI: 10.48550/arXiv.2307.14302

CITATIONS

0

READS

170

6 authors, including:



Eirik Valseth

Norwegian University of Life Sciences

53 PUBLICATIONS 146 CITATIONS

[SEE PROFILE](#)



Clint Dawson

University of Texas at Austin

338 PUBLICATIONS 12,557 CITATIONS

[SEE PROFILE](#)

A Discontinuous Galerkin Finite Element Model for Compound Flood Simulations

Chayanon Wichitrnithed^{a,*}, Eirik Valseth^{a,b,c}, Ethan J. Kubatko^d, Younghun Kang^d,
Mackenzie Hudson^d, Clint Dawson^a

^a*The Oden Institute for Computational Engineering and Sciences, The University of Texas at Austin, 201
E. 24th St. Stop C0200, Austin, 78712, Texas, United States of America*

^b*The Department of Data Science, The Norwegian University of Life Science, Drøbakveien
31, Ås, 1433, Norway*

^c*Department of Scientific Computing and Numerical Analysis, Simula Research Laboratory, Kristian
Augusts gate 23, Oslo, 0164, Norway*

^d*The Department of Civil, Environmental, and Geodetic Engineering, The Ohio State University, 2070 Neil
Ave, Columbus, 43210, Ohio, United States of America*

Abstract

Recent tropical cyclones, e.g., Hurricane Harvey (2017), have lead to significant rainfall and resulting runoff with accompanying flooding. When the runoff interacts with storm surge, the resulting floods can be greatly amplified and lead to effects that cannot be modeled by simple superposition of its distinctive sources. In an effort to develop accurate numerical simulations of runoff, surge, and compounding floods, we develop a local discontinuous Galerkin method for modified shallow water equations. In this modification, nonzero sources to the continuity equation are included to incorporate rainfall into the model using parametric rainfall models from literature as well as hindcast data. The discontinuous Galerkin spatial discretization is accompanied with a strong stability preserving explicit Runge Kutta time integrator. Hence, temporal stability is ensured through the CFL condition and we exploit the embarrassingly parallel nature of the developed method using MPI parallelization.

We demonstrate the capabilities of the developed method though a sequence of physically relevant numerical tests, including small scale test cases based on laboratory measurements and large scale experiments with Hurricane Harvey in the Gulf of Mexico. The results highlight the conservation properties and robustness of the developed method and show the potential of compound flood modeling using our approach.

Keywords: Hurricane Storm Surge, Compound Flooding, Hurricane Harvey,
Discontinuous Galerkin

*Corresponding author

Email address: namo@utexas.edu (Chayanon Wichitrnithed)

1. Introduction

In this paper, we present recent advances and developments of discontinuous Galerkin (DG) finite element (FE) methods in shallow water flows in coastal, riverine, and overland flows. In particular, we focus on the application of DG methods to the shallow water equations (SWE) for flood events in which hurricane storm surge interacts with one or more other sources of water, i.e., compound flood events [1]. Modeling these events in coastal regions remains a significant challenge as the number of physical processes that play a role are significant, e.g., storm surge, river discharge, tides, rainfall, and winds. As noted by multiple researchers, these processes typically interact in a highly nonlinear fashion and require careful treatment to ensure accurate modeling [2, 3, 4, 5]. Our approach to this modeling challenge is the development of a comprehensive DG solver which computes FE approximations to modified SWE with nonzero source terms in a single domain covering ocean, rivers, and overland areas. Hence, in this work, we focus on compound flooding from the following sources: storm surge, river runoff, and rainfall.

Flooding from each of the sources has been extensively studied, and there are numerous models in existence. Here, we do not aim to provide a complete list here but mention some well-established and commonly used models. For storm surge, the AAdvanced CIRCulation (ADCIRC) model [6, 7], the Sea, Lake, and Overland Surges from Hurricanes (SLOSH) [8], and Delft3D [9] have all been extensively validated for past hurricane events. In addition, there are also a significant number of validated models for riverine and rain-induced overland flows, such as the Hydrologic Engineering Center River Analysis System (HEC-RAS) model [10, 11] and the Gridded Surface Hydrological Analysis (GSSHA) model [12]. These two sets of models are typically applied over vastly different scales, from watershed scale to global ocean scale and are thus, generally, not used in overlapping domains.

A significant portion of current modeling efforts of compound flooding are based on coupling existing models for individual physical processes, see [3] for a comprehensive review. The methodologies for coupling such models can be vary in complexity from simple one-way coupling in which input from one model is the output from another, to fully coupled multi-physics models in which all governing physics are resolved simultaneously. The models of lower complexity typically consist of well established, validated models for each individual flood component. However, recent work utilizing the aforementioned surge models, e.g., by Loveland *et al.* [2] has shown the applicability of the ADCIRC model in modeling interactions between riverine flows and storm surge through careful construction of the FE mesh and model inputs.

To model compound flooding, we rely on the SWE as the governing model. The SWE are a set of nonlinear transient partial differential equations (PDEs), and thus, analytic solutions cannot be established for cases beyond that of academic interest. Hence, accurate numerical approximation is critical. Current (physics-based) modeling efforts based on numerical approximation of transient PDEs such as the SWE can broadly be categorized to be of FE, finite volume (FV), and finite difference (FD) approximations for the spatial differential operators. In general, the temporal differential operators are discretized using implicit, explicit, or a combination of implicit and explicit FD schemes. Space-time approaches in which both spatial and temporal operators are discretized using FE methods also exist, see, e.g., [13]. However, due to the computational cost of such approaches these are generally

not used in large-scale shallow water modeling. In our approach to model compound flooding from surge, runoff, and rainfall, we employ the previous work on explicit-in-time DG methods for SWE by Kubatko *et al.* [14] and Dawson *et al.* [15]. DG methods are chosen as they possess several features making them very well suited to solve the SWE, including: local conservation, unstructured meshes, p -adaptivity, ease of parallelization, etc. [16].

One critical addition to the DG model in this work is rainfall in the form of a source term appearing in the depth-averaged continuity equation of the SWE (see Equation (1) of the next section). Two methods of approximating the rainfall term are explored here. One approach is the direct interpolation of rainfall rates onto the mesh from observed rainfall data, which are available from a number of sources at various spatial and temporal resolutions (see [17] for a comprehensive overview of precipitation data sets). A second approach, applicable during tropical cyclones (TCs), is the implementation of a parametric rainfall model directly within the DG model. This approach takes advantage of the fact that, during TCs, rainfall patterns in the vicinity of the storm exhibit defined structures that can be exploited by a parametric model, which uses simple analytic expressions based on a small number of (predicted or observed) storm parameters that are made publicly available by the National Hurricane Center pre and post storm events. This type of approach is already implemented in our DG model for constructing wind fields during TCs and provides an existing code infrastructure that can be leveraged for computing rainfall rates.

In the following, we introduce, verify, and validate our compound flood modeling methodology. In section 2, we introduce the governing model PDE, modified to account for rainfall. In this section, we also introduce the DG discretization of the SWE and the parametric rainfall models used to generate rainfall source data. In addition, we provide an overview of the implementation details as well as other recent additions to the numerical model we employ. Next, in Section 3, we present a comprehensive verification and validation of our methodology including benchmark tests of conservation properties as well as large scale hurricanes with compound flood effects. Finally, in Section 4, we draw conclusions and discuss potential future research directions.

2. Governing Equations and DG Formulation

The DG formulation and solution method used within our framework is based on the previous works [14, 15]. Hence, we do not include a comprehensive introduction to the details of the formulation but rather a brief overview to make this presentation sufficiently self contained. The governing model we use for shallow water flow are the two-dimensional SWE which consist of the conservative depth-averaged equations of mass conservation as

well as x and y momentum conservation [18]:

Find (ζ, \mathbf{u}) such that:

$$\begin{aligned} \frac{\partial \zeta}{\partial t} + \operatorname{div}(H\mathbf{u}) &= R, \text{ in } \Omega, \\ \frac{\partial(Hu_x)}{\partial t} + \operatorname{div}\left(Hu_x^2 + \frac{g}{2}(H^2 - h_b^2), Hu_x u_y\right) - g\zeta \frac{\partial h_b}{\partial x} + \tau_b Hu_x &= F_x, \text{ in } \Omega, \\ \frac{\partial(Hu_y)}{\partial t} + \operatorname{div}\left(Hu_x u_y, Hu_y^2 + \frac{g}{2}(H^2 - h_b^2)\right) - g\zeta \frac{\partial h_b}{\partial y} + \tau_b Hu_y &= F_y, \text{ in } \Omega, \end{aligned} \quad (1)$$

where ζ is the free surface elevation above the geoid, h_b the bathymetry, H is the total water column (see Figure 1 for definition of these three quantities), $\mathbf{u} = \{u_x, u_y\}^T$ is the depth-averaged velocity field, τ_b is the bottom friction factor, R is the rainfall rate, and the source terms F_x, F_y represent potential relevant sources which induce flow, including, e.g., Coriolis force, tidal potential forces, wind stresses, and wave radiation stresses. Ω is the computational domain, e.g., the coastal ocean, and its boundary Γ is identified by three distinctive sections $\Gamma = \Gamma_{ocean} \cup \Gamma_{land} \cup \Gamma_{river}$.

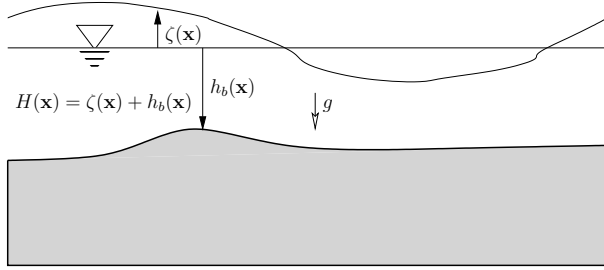


Figure 1: Definition of shallow water elevations.

The PDEs (1) differs from the previous works [14, 15] in the inclusion of the (potentially nonzero) right hand side of the mass conservation equation, the rainfall rate R . To complete an initial boundary value problem (IBVP), (1) is augmented with proper initial and boundary conditions. In addition to the open ocean (specified elevation) and land boundary condition (zero normal flow) used in [15], we have river flow (specified normal flow) boundaries:

$$\mathbf{u} \cdot \mathbf{n} = q_{river} \text{ on } \Gamma_{river}, \quad (2)$$

where q_{river} are the specified river flows of unit m^2/s .

By defining the vector of unknowns $\mathbf{w} = \{\zeta, Hu_x, Hu_y\}^T$, the source vector \mathbf{s} and the flux matrix $\mathbf{F}(\mathbf{w})$ as:

$$\begin{aligned} \mathbf{w} &= [\zeta, uH, vH]^T \\ \mathbf{s} &= \left[R, g\zeta \frac{\partial h_b}{\partial x} + F_x, g\zeta \frac{\partial h_b}{\partial y} + F_y \right]^T \end{aligned}$$

$$\mathbf{F}(\mathbf{w}) = \begin{bmatrix} uH & vH \\ Hu^2 + g(H^2 - h_b^2) & Huv \\ Huv & Hv^2 + g(H^2 - h_b^2) \end{bmatrix}$$

we can write the three equations in the form

$$\frac{\partial \mathbf{w}}{\partial t} + \nabla \cdot \mathbf{F}(\mathbf{w}) = \mathbf{s}, \quad i = 1, 2, 3. \quad (3)$$

The corresponding weak formulation is obtained by multiplying each equation by a test function \mathbf{v} and integrating over each element e , and subsequent integration by parts:

$$\left(\frac{\partial \mathbf{w}}{\partial t}, \mathbf{v} \right)_{\Omega_e} - (\nabla \mathbf{v}, \mathbf{F})_{\Omega_e} + \langle \hat{\mathbf{F}} \cdot \mathbf{n}, \mathbf{v} \rangle_{\partial \Omega_e} = (\mathbf{s}, \mathbf{v})_{\Omega_e} \quad (4)$$

where $\hat{\mathbf{F}}$ represents a choice of numerical flux. The solution \mathbf{w} is then spatially approximated as \mathbf{w}_h using an orthogonal Dubiner basis ϕ_{ij} as:

$$\mathbf{w}_h = \sum_i \sum_j \tilde{\mathbf{w}}_{ij} \phi_{ij} \quad (5)$$

where $\tilde{\mathbf{w}}_{ij}$ are the modal degrees of freedom. Substituting this into the weak formulation above as well as an identical choice for the test function \mathbf{v} reduces the problem to a system of ODEs in the form:

$$\frac{d}{dt}(\mathbf{w}_h) = L_h(\mathbf{w}_h), \quad (6)$$

where the terms from (4) are collected into L_h . We then use an optimized, explicit Strong Stability Preserving Runge-Kutta scheme (SSPRK) [19], based on Shu and Osher [20, 21] to discretize (6) in time and compute the difference approximation \mathbf{w}_h^{n+1} , at the next timestep.

2.1. Implementation

To implement the SSPRK DG-method of our SWE, we extend the numerical model DG-SWEM (Discontinuous Galerkin Shallow Water Equation Model) first developed as part of [14]. The code is parallelized through MPI and is compatible with meshes and inputs developed for ADCIRC. In the implementation, p -order DG approximations as introduced above are available with several choices for the numerical flux $\hat{\mathbf{F}}$, an advanced wetting and drying algorithm [22], as well as an optional slope limiter that can be applied in cases where shocks arise.

The basic procedure of the code is outlined in Figure 2. The spatial discretization of the DG formulation is local to each element; that is, the approximation of the integral terms appearing in (6) can be performed element-by-element without having to solve a global mass matrix system as in the Bubnov-Galerkin method. Specifically, we first compute the edge integrals $\langle \hat{\mathbf{F}} \cdot \mathbf{n}, v \rangle_{\partial \Omega_e}$ of each element and then the area integrals $(s, v)_{\Omega_e} + (\nabla v, \mathbf{F})_{\Omega_e}$ of each element.

The entry point for rainfall is nodal, i.e. rain intensity r will have to be specified at each node in the grid. For example, it could be spatially interpolated from historical data or

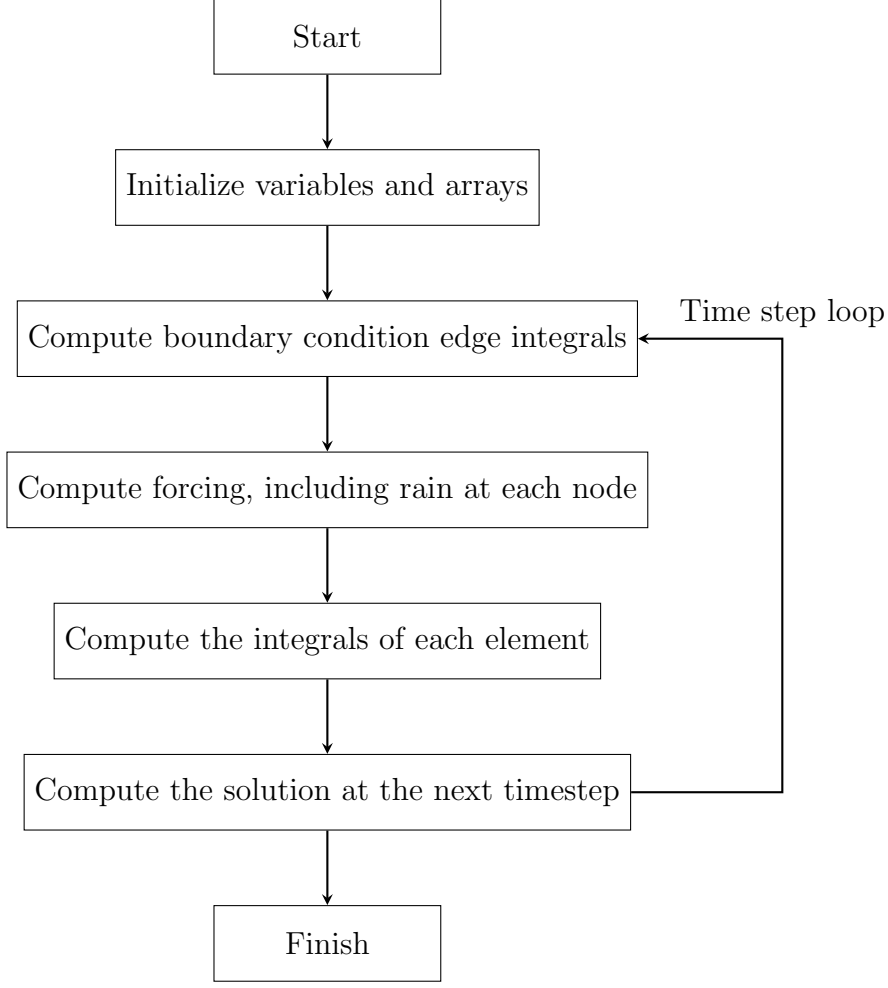


Figure 2: Flowchart of DG-SWEM

estimated using *parametric models* as discussed in the next section. To transform the nodal rain intensity to the elemental source term r we simply compute the average rain intensity, i.e. in the term $(R, v)_{\Omega_e}$ we have

$$R = \frac{R(n_e^1) + R(n_e^2) + R(n_e^3)}{3} \quad (7)$$

where n_e^1, n_e^2, n_e^3 are the nodes of element e . Note that this term is added for all elements, whether wet or dry. This allows dry elements to become eventually wet from the rain and not only from mass transfer from neighboring elements.

Apart from the addition of rainfall forcing into the DG-SWEM codebase, we have also added the capability of transient river boundary conditions as (2). In practice, these are prescribed by properly selecting the numerical $\hat{\mathbf{F}}$ for the element edges that are river boundaries. The final point of which we have improved the capabilities of DG-SWEM is the incorporation of a new parametric hurricane wind and pressure field model called the Generalized Asymmetric Holland Model (GAHM). This parametric model is based on the classical Holland Model [23] and has been designed specifically to handle ADCIRC hurricane input.

These parametric models use National Hurricane Center (NHC) forecasts (or hindcasts after the hurricanes have dissipated) which includes time series data such as storm track, central pressure, and maximum winds. We refer to the ADCIRC Wiki page¹ for further details on the GAHM.

2.2. Rainfall Data

To ascertain the rainfall intensity needed in (7), we essentially have two options: forecast rainfall data from atmospheric models and observed and spatially interpolated rainfall data available post rain or storm event. As an overarching goal of the present work is to develop numerical compound flood models that are capable of forecasting, post event observed data is less relevant. However, for validation and hindcasting purposes, high quality post-event rainfall data is critical.

During tropical cyclones, rainfall patterns in the vicinity of the storm exhibit defined structures that can be exploited by so-called parametric rainfall models. The basic idea behind this approach is to construct rainfall fields using simple analytic expressions based on a small number of (predicted or observed) storm parameters that are made publicly available by the NHC pre and post storm events. This type of approach has been implemented in DG-SWEM based on the so-called R-CLIPER (Rainfall CLImatology and PERsistence) model, which computes rainfall rates $R(r)$ within a radius r of the storm center as summarized in Figure 3; see [24] for more details. Note that the primary inputs of the model are the reported storm centers and maximum wind velocities, which are generally provided at 6-hour intervals by the NHC. Within DG-SWEM, linear interpolation is used to obtain the storm parameters at the model time step, and the rainfall rate at each finite element mesh node is computed based on its radial distance from the storm center.

Alternatively, the program accepts observed rainfall data in hindcasting scenarios in the GRIB2 format which is read during each timestep. As this type of data is given with spatially varying distributions over the nation, this data is readily interpolated onto finite element meshes.

3. Numerical Experiments and Evaluation

In this section we present a series of numerical experiments designed to verify and validate the developed numerical model. First, a test case in a simple rectangular geometry which is designed to test the conservation properties of the method. Second, a test case from literature for rainfall onto an inclined plane to compare to laboratory experimental data. Third, we perform a large-scale test case corresponding to Hurricane Harvey (2017). Last, an alternative compound flood approach commonly used in ADCIRC where runoff data is incorporated through river source terms in a domain covering the Neches River, Texas. In all cases, we employ a similar set-up of the solver using Manning's friction law, linear discontinuous approximation functions, Roe flux, and a two-stage, second order SSPRK scheme. The only exception is the Hurricane Harvey case for which we use the Local Lax-Friedrichs Flux and a five-stage, second order SSPRK scheme.

¹https://wiki.adcirc.org/Generalized_Asymmetric_Holland_Model#cite_note-1

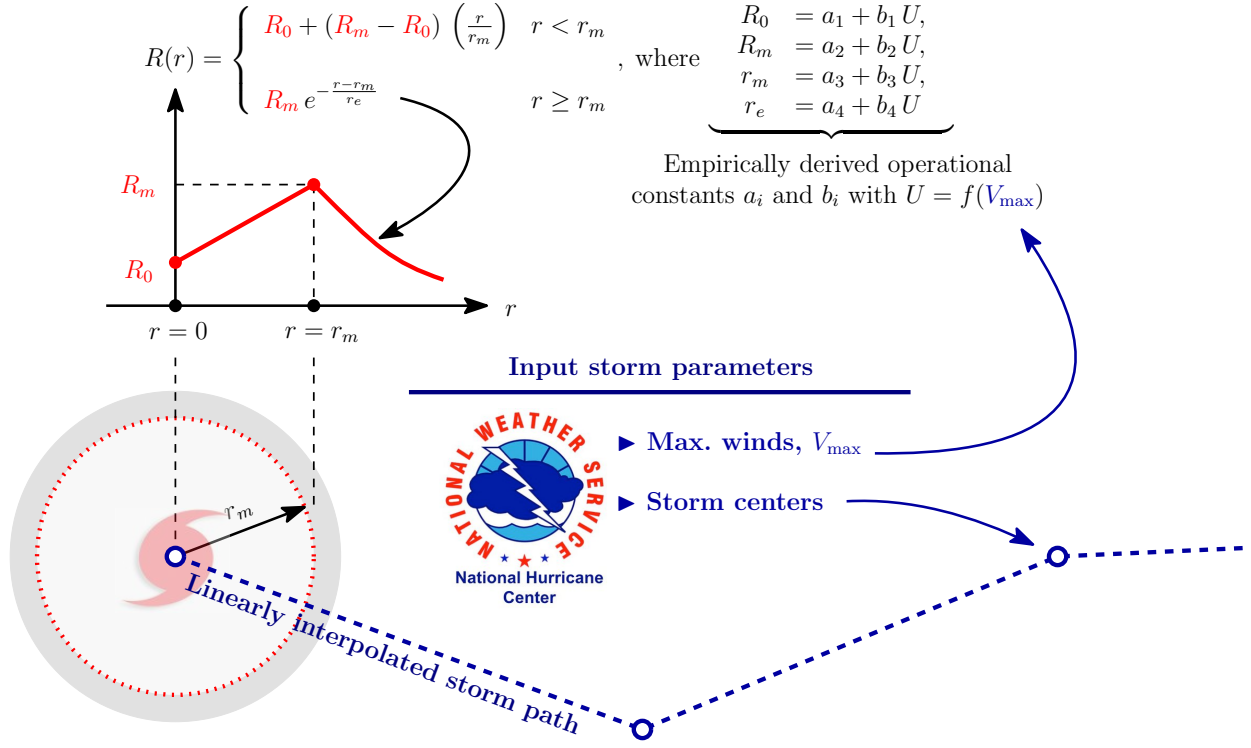


Figure 3: Illustration summarizing the R-CLIPER parametric rainfall model, which computes rainfall rate $R(r)$ at a radius r from a given storm center using the expressions shown. The primary inputs to the model are the reported maximum wind velocities, V_{\max} , and the storm centers, which are generally provided at 6-hour intervals by the National Hurricane Center (NHC).

3.1. Filling a “Bathtub”

As an initial numerical experiment we verify the well-balanced nature of our DG solver in the presence of nonzero source terms. We accomplish this by considering a modification of the classical lake-at-rest test case [25]. Hence, we consider a rectangular domain $(0, 50000m) \times (0, 8000m)$ with bathymetry:

$$h_b(x, y) = 5 - e^{-100(x-25000m)^2}, \quad (8)$$

see Figure 4. We assume that the bottom is uniform and has a constant quadratic friction

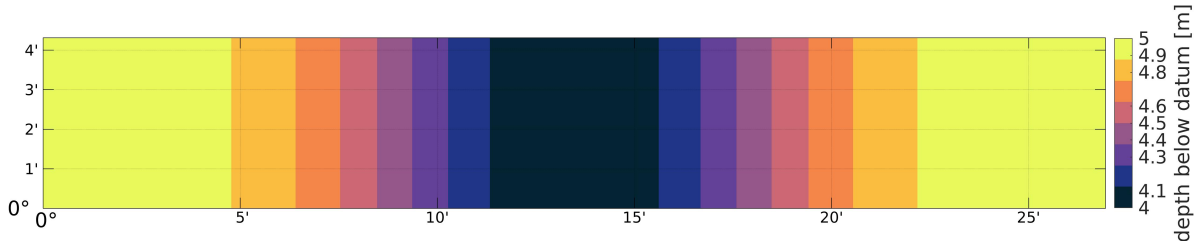


Figure 4: Bathymetry of the bathtub mesh.

coefficient of 0.001, set the time step size to 5 seconds, and apply zero-flow boundary conditions on all domain edges. We incorporate a constant rainfall rate of 7.0556×10^{-6} m/s (1 inch/hour) for 24 hours, followed by 48 hours of no forcing. At the conclusion of the simulation, the water surface elevation is reported to be 0.6096 m, an exact match when computing the volume added by the constant rainfall. Lastly, the maximum velocity throughout the simulation is 0.35×10^{-13} m/s. Hence, we conclude that the inclusion of rainfall into the DG solver does not disturb the well-balanced property.

3.2. Rain on Inclined Plane

With this test case, we validate the ability of DG-SWEM to accurately simulate rainfall runoff on an (initially dry) inclined plane subjected to rainfall rates of varying duration. Specifically, computed water depths and outflow discharges are validated against a set of well-known experimental results from Iwagaki [26], which have been used in a number of validation studies; see, for example, [27, 28, 29].

Figure 5 shows the two experimental “conditions” investigated by Iwagaki, both of which used a 24 m-long aluminum flume (Manning coefficient of $n = 0.009$, as reported by Iwagaki) having a rectangular cross section of 19.6 cm width and 9 cm depth. In condition (A), the flume was set at a uniform slope of $\sin \theta = 0.015$ and subjected to a uniform rainfall rate of $R = 0.0833$ cm/s. In condition (B), the flume was set (from top to bottom) at slopes of $\sin \theta = 0.020, 0.015$, and 0.010 and subjected to rainfall rates of $R = 0.1080$ cm/s, 0.0638 cm/s, and 0.0800 cm/s, respectively, with each segment being 8 meters long. For both conditions, rainfall rates of time duration $T = 10, 20$, and 30 seconds were investigated and measurements of the water depth and discharge were reported at the end of the flume.

Each 8-m segment of the flume is discretized as shown in the inset of Figure 5. Numerical simulations for both conditions (A) and (B) were performed with DG-SWEM for each of the three rainfall durations, $T = 10, 20$, and 30 seconds, using piecewise polynomial spaces of degree $p = 1$. As reported by Iwagaki, Manning’s coefficient was set to $n = 0.009$ (no model calibration was performed), and numerical simulations were run for a total of 86.4 seconds using a time step of $\Delta t = 0.001$ seconds. Figures 6 and 7 show the computed water depth and outflow discharge at the end of the flume obtained from the DG-SWEM simulation compared to Iwagaki’s experimental results for conditions (A) and (B), respectively. Overall, it can be observed that the DG-SWEM results closely match the experimental measurements, with computed output accurately reproducing the rising and recession limbs of the hydrographs. Additionally, in general, the peak water depth and discharge values, and the time at which these peaks occur, are well captured with the model. For example, the root-mean-square error in peak water depths under condition (B) is only 0.06 cm.

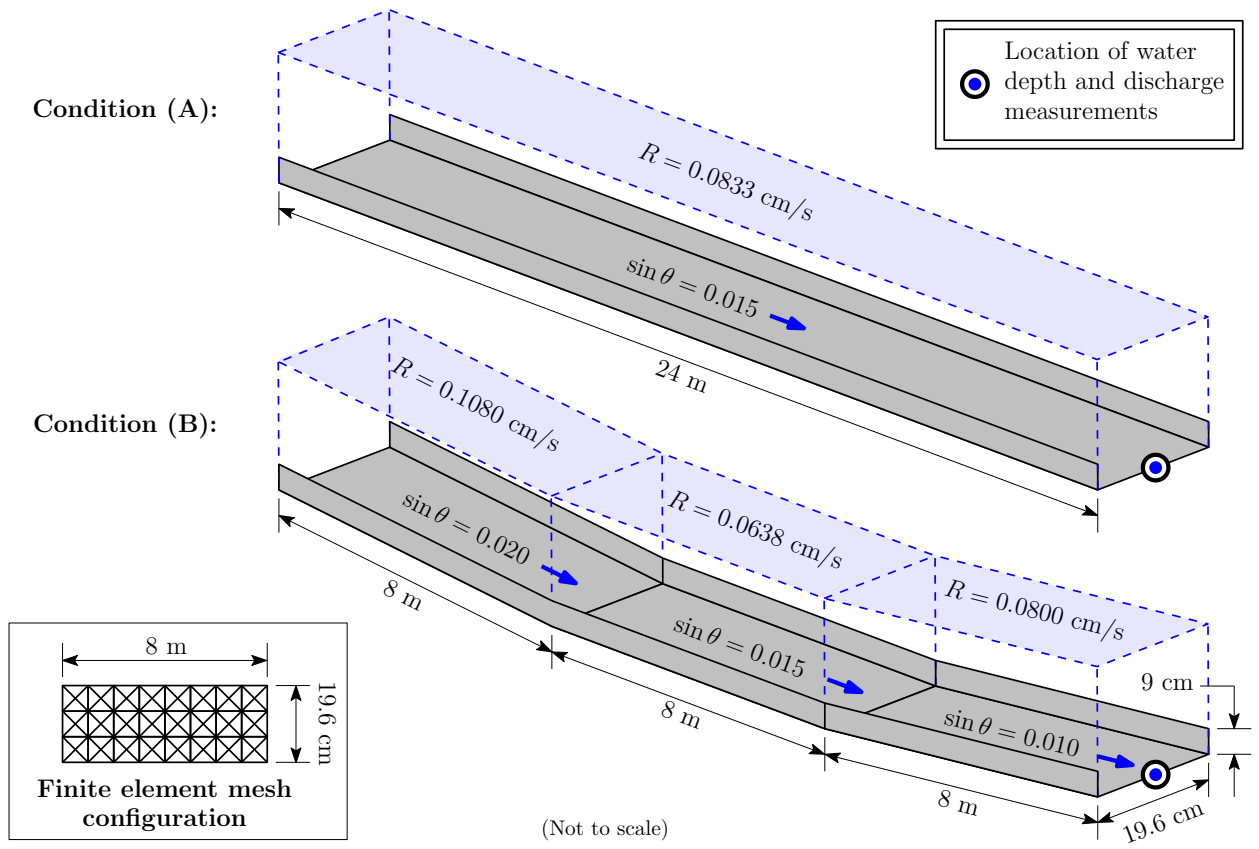


Figure 5: Iwagaki's experimental setup for conditions (A) and (B) with rainfall rates, R , as shown for time durations of $T = 10, 20$, and 30 seconds. Bottom inset shows the finite element mesh configuration used for simulation.

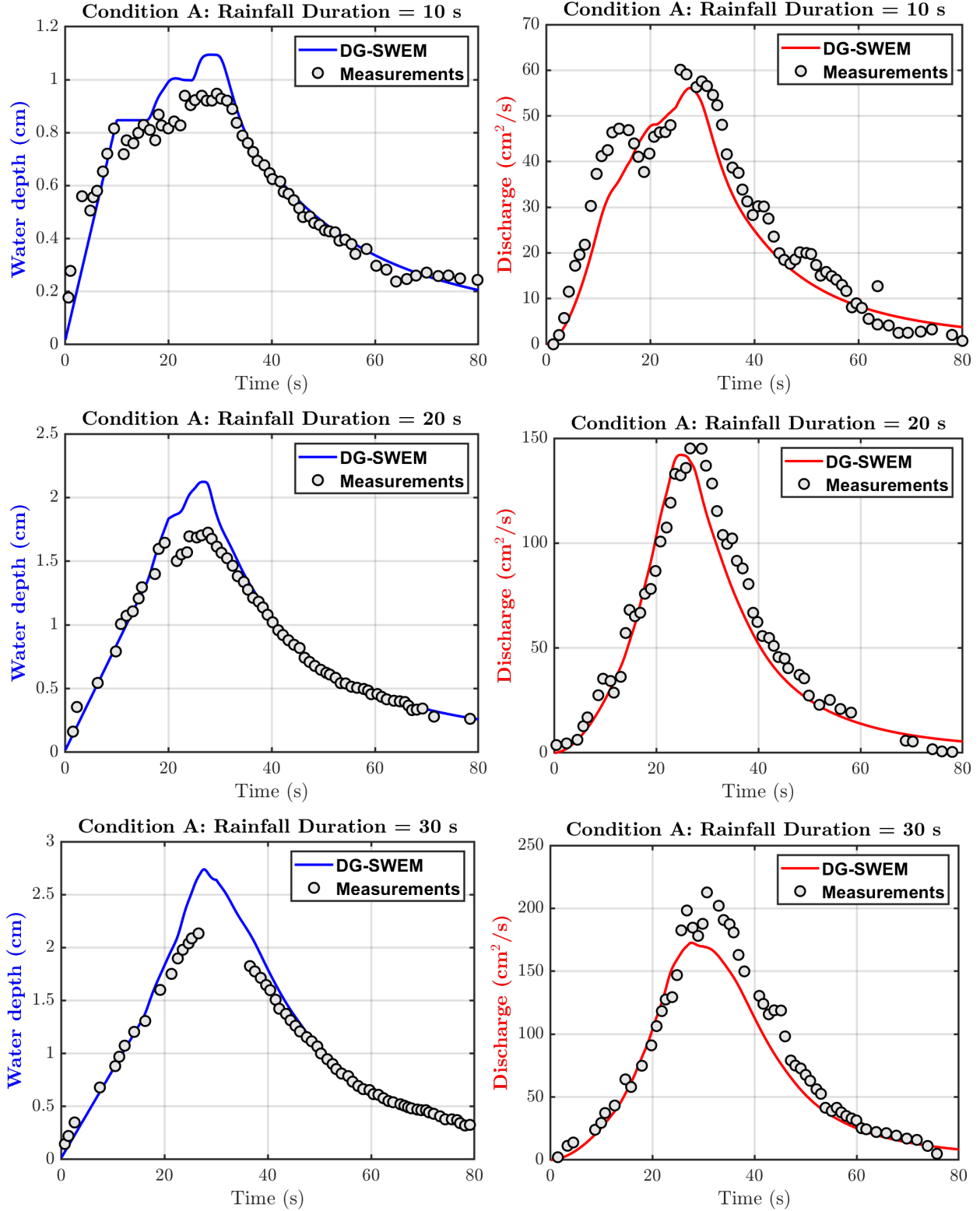


Figure 6: Plots for Iwagaki's “Condition (A)” comparing DG-SWEM results for water depth (left, blue) and discharge (right, red) to Iwagaki's measurements (gray circles) at the end of the 24-m flume. Rainfall durations are 10, 20, and 30 seconds (top, middle, and bottom, respectively).

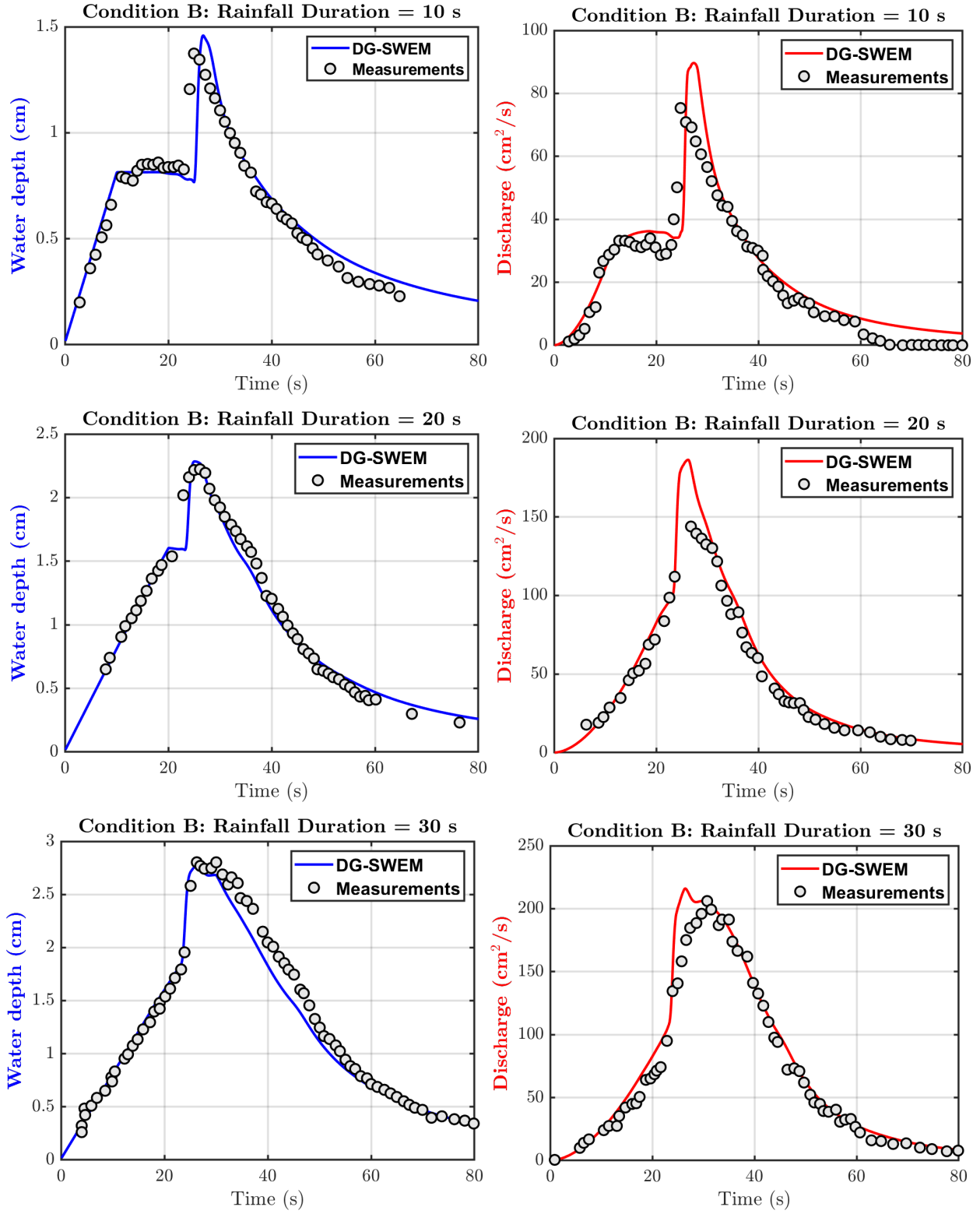


Figure 7: Plots for Iwagaki's "Condition (B)" comparing DG-SWEM results for water depth (left, blue) and discharge (right, red) to Iwagaki's measurements (gray circles) at the end of the 24-m flume. Rainfall durations are 10, 20, and 30 seconds (top, middle, and bottom, respectively).

3.3. Hurricane Harvey

As a final validation test, we consider a canonical case of compound flooding, Hurricane Harvey (2017). During the storm, moderate surge in Galveston Bay compounded with more than 50 inches of total rain in the Houston area [30] and induced historic floods in the Houston area. Hurricane Harvey made its initial landfall on August 25th 2017 on San José island [31], before moving into the Gulf of Mexico before its second landfall near the Texas-Louisiana border two days later, see Figure 8 for its track in the Gulf of Mexico. Between these landfalls, the storm system moved back into The Gulf of Mexico and lead to extreme rainfall in Houston and surrounding areas.

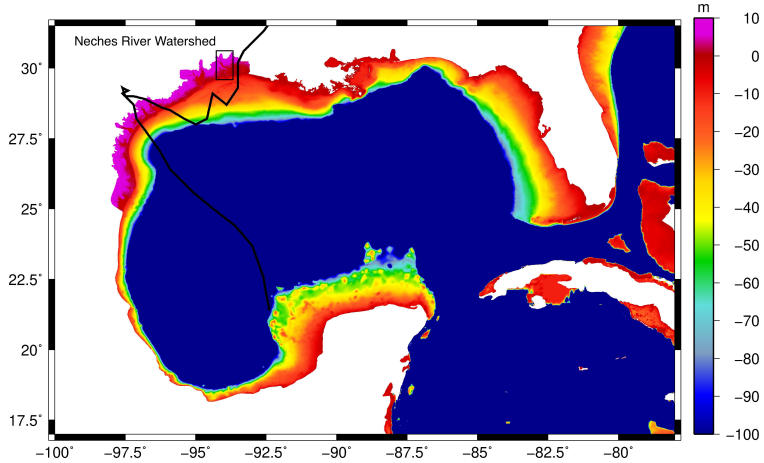


Figure 8: Track of Hurricane Harvey in the Western Gulf of Mexico. Note that the color scale represents bathymetry.

To perform simulations of the floods during Hurricane Harvey using the developed DG solver, we rely on established and validated inputs for Hurricane storm surge modeling using ADCIRC presented in [32]. The inputs include an unstructured mesh consisting of 3,352,598 nodes distributed among 6,675,517 triangular finite elements, shown in Figure 9, as well as spatially variable descriptions of Manning's n . In addition to bathymetry and bottom friction, the inputs also include parametrizations and descriptions of tides, levees, and wind-inhibiting vegetation along the Texas coast.

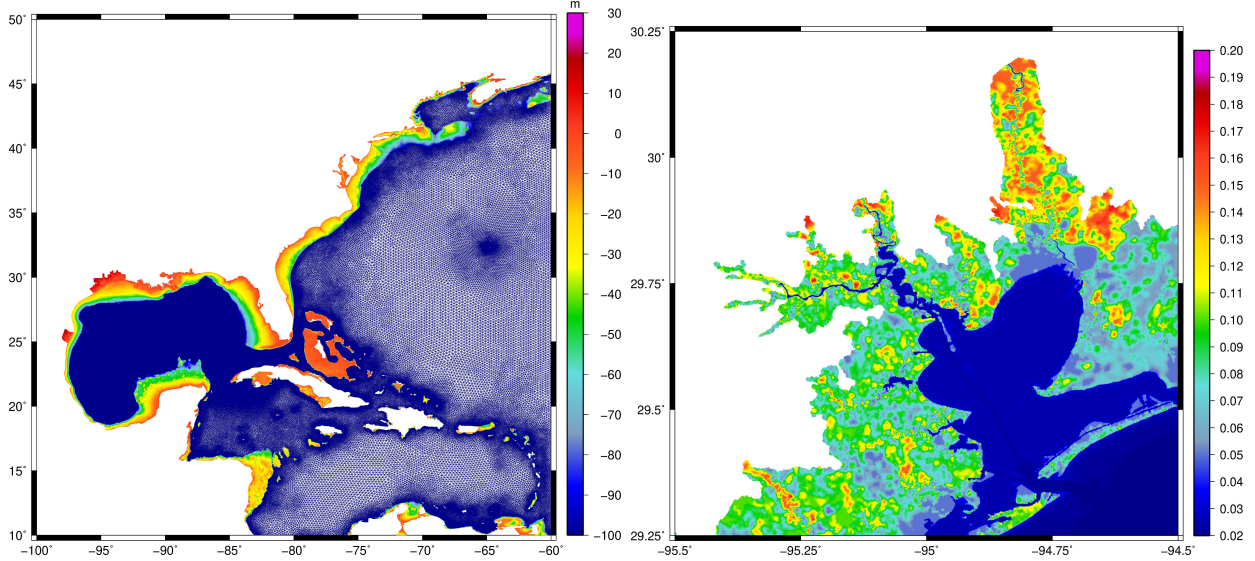


Figure 9: (Left) Bathymetry of the mesh. (Right) Zoomed-in portion of the mesh showing Manning’s n values in the Galveston Bay area.

To emulate the process and data stream in a forecasting scenario, we obtain Best Track data from the National Hurricane Center HURDAT2 database [33]. As in [32], we perform a tidal spinup without winds to ensure stability and accuracy of the model once hurricane strength winds are applied. The 30-day spinup is followed by a run from August 23 to September 2, 2017 during which Harvey made landfall, and hurricane winds and rainfall are incorporated using the GAHM and the R-CLIPER model, respectively. To ensure stability of the temporal discretization we use a timestep of 0.5 seconds. This fine resolution in both space and time leads to a runtime of approximately 13 hours with 3,200 processors on the Frontera supercomputer at The Texas Advanced Computing Center.

To compare the results, we consider three simulation cases: a surge-only case with no rainfall, a case using the R-CLIPER model, and a case with observed rainfall intensity data from Iowa State weather data archive [34]. This gridded data is interpolated onto the mesh to obtain rain forcing in (7). In Figure 11, we present a comparison of water elevation output from these cases to observed gauge data at several NOAA stations near the area where Harvey made its initial Texas landfall. This area is shown in Figure 10.

In all gauges we notice an underprediction of the water surface elevation compared to the measured data, however, the added rainfall clearly increases the elevation at all considered locations. We do notice some discrepancy between the results using R-CLIPER and the interpolated observed rainfall. This is not surprising as the two sources are fundamentally different, and the quality of the hindcast data may not be perfect in all locations. The gauges presented in Figure 11 were selected as they all are near the location of Hurricane Harvey’s first landfall on the Texas coast and all represent locations where the addition of the parametric rainfall source made the model predictions closer to the measured gauge data. In Locations closer to Houston where the majority of the compound floods occurred, the parametric R-CLIPER model made nearly no difference compared to the surge only case. The reason can be deduced by inspecting the model in Figure 3 and the track of Hurricane Harvey in Figure 8. Since the eye of the hurricane passed very far off the coast,

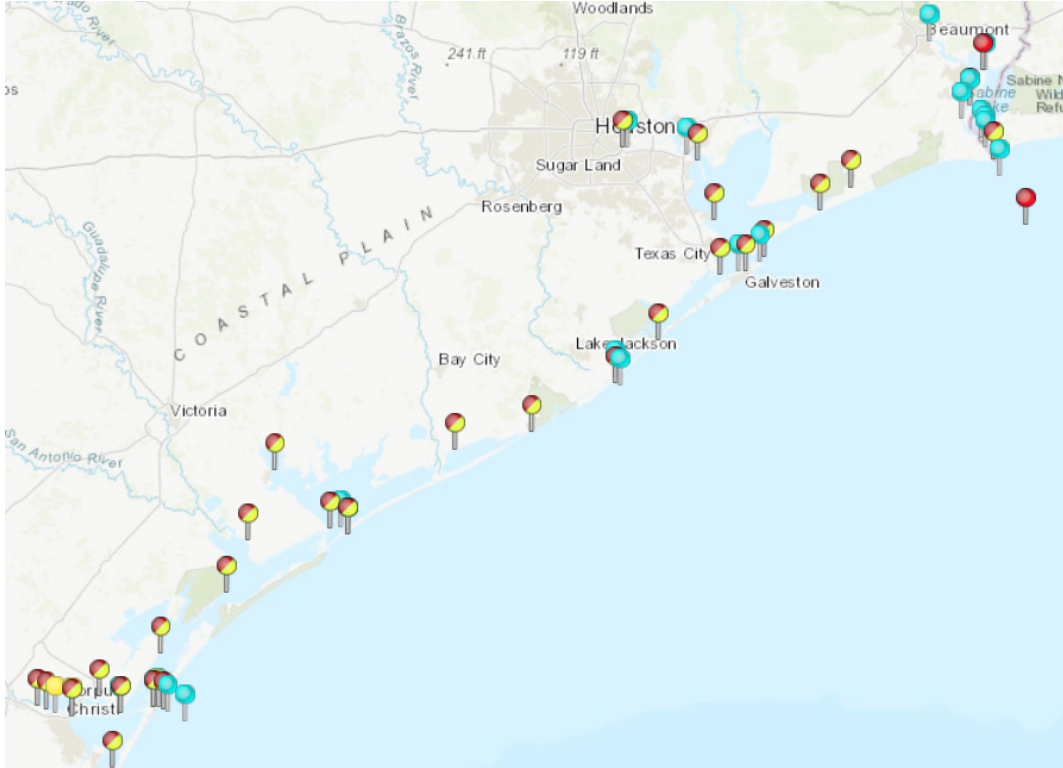


Figure 10: NOAA stations in the region where Harvey made landfall. Plot obtained from <https://tidesandcurrents.noaa.gov/map/>

the contribution from R-CLIPER in the Houston area was vanishingly small.

To further investigate the results with rainfall from R-CLIPER, we compare in Figure 12 the high water mark measurements from runs with and without parametric rainfall. Points within a 200 km radius of landfall were chosen, and their observed values were obtained from USGS [35]. The corresponding values from DG-SWEM were interpolated from the nodal max elevation values. These results present two interesting features: *i*) while including more points that become wet and severely flood, the incorporated rainfall also introduces more outliers in the data, *ii*) the R^2 value is noticeable increased when including rainfall but the RMSE is also increased.

3.4. Neches test case

The final test case is based on the approach to compound flood modeling presented in [2], focused here on river-coastal ocean interaction. In this case, we consider the Lower Neches River watershed near the Texas-Louisiana border, see Figure 8. During Hurricane Harvey, this watershed was subjected to extreme rainfall and large portions of its surrounding areas were inundated during and after the event. This event was also studied using ADCIRC and compared to HEC-RAS in [2] and the present study is based on preserved inputs from Loveland *et al.*. We only present key features of this model and refer readers to the original publication for greater detail. The model domain has been extracted from the ADCIRC inputs used in the preceding section and contains 122,839 elements and 62,075 nodes and the domain is shown in Figure 13.

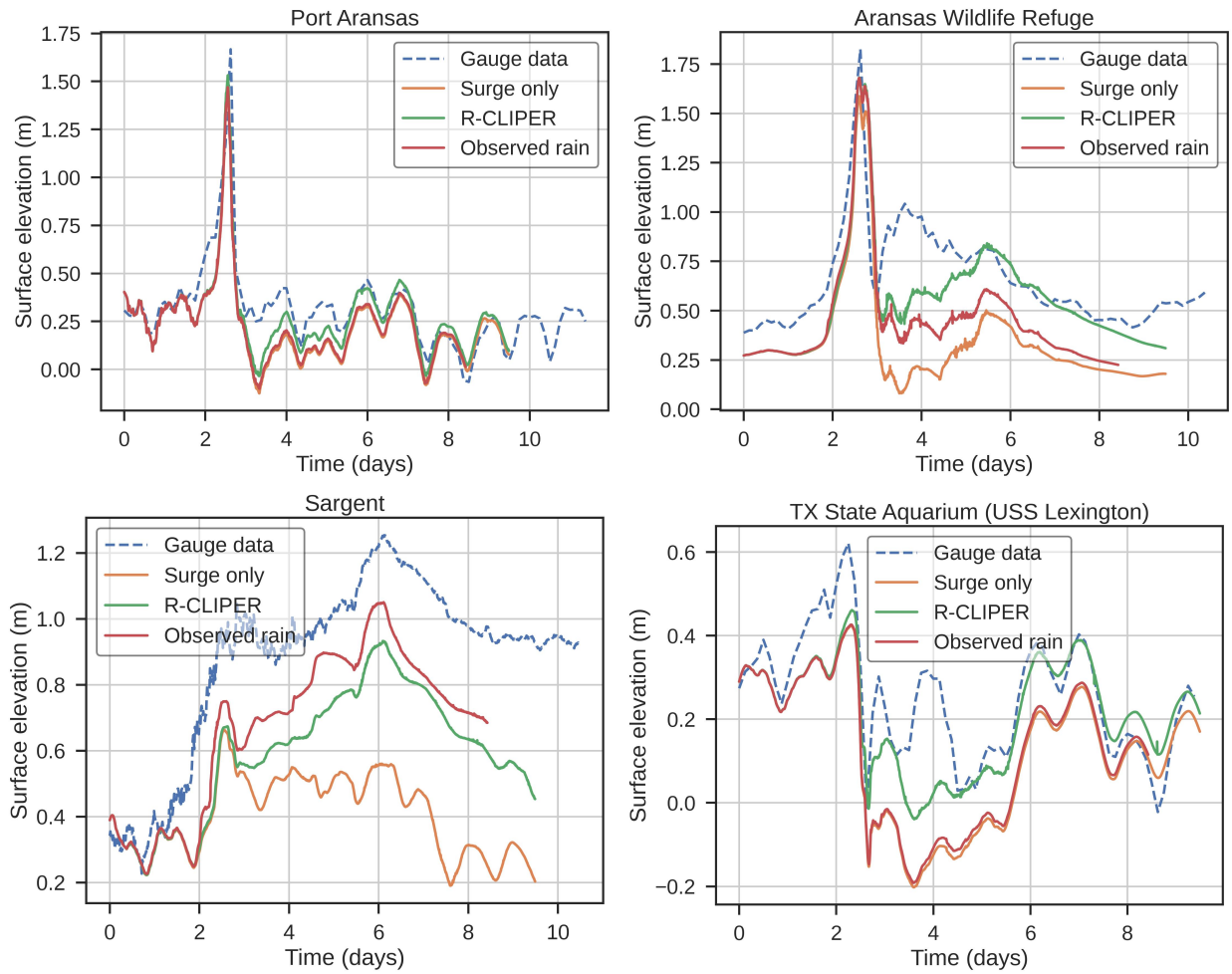


Figure 11: Water elevation comparisons between a run without any rain (orange), one using parametric rainfall (green), one using observed rain data (red), and NOAA station measurements (dashed blue). Time is relative to the starting date 8/23/2017.

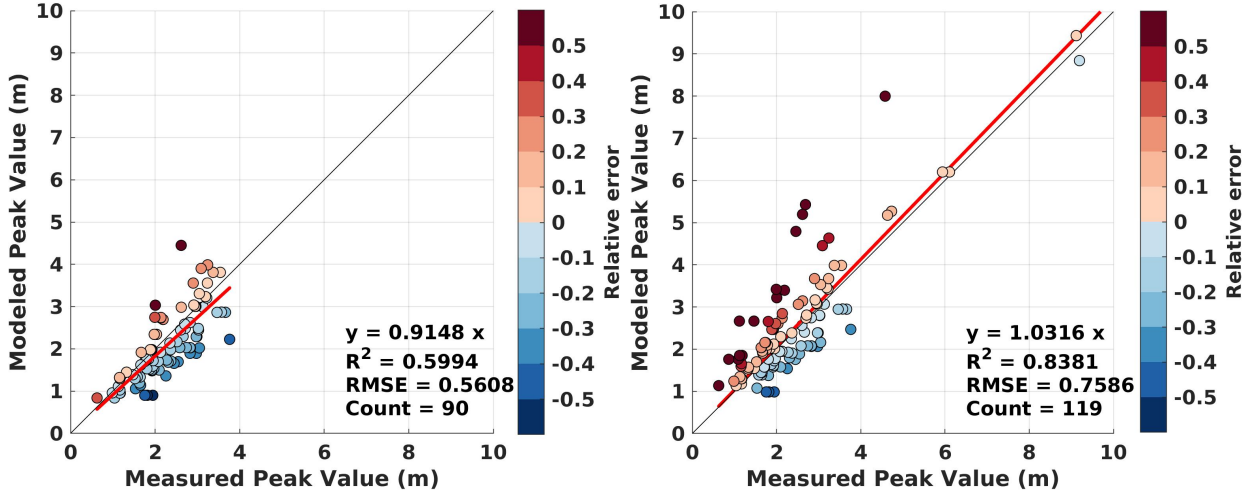


Figure 12: High water mark comparison for Hurricane Harvey. The left plot shows a run without any rain, while the right shows a run using the R-CLIPER parametric rainfall model.

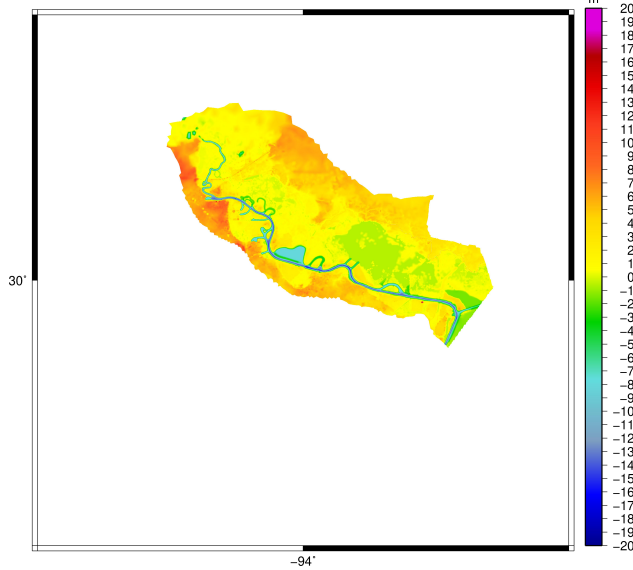


Figure 13: Bathymetry of the Neches River domain.

Hence, the highly detailed unstructured mesh, bathymetry and topography, as well as parameters such as Manning's n are preserved. To force the model, river flow data was extracted from a validated HEC-RAS model and a USGS gauge. At the downstream end of the river which terminates into Sabine Lake, an elevation boundary condition was applied based on the same HEC-RAS model and a NOAA gauge.

To compare results from our current DG model and ADCIRC, we use the preserved inputs and run both models. The time frame in these figures is August 20 to September 1, 2017.

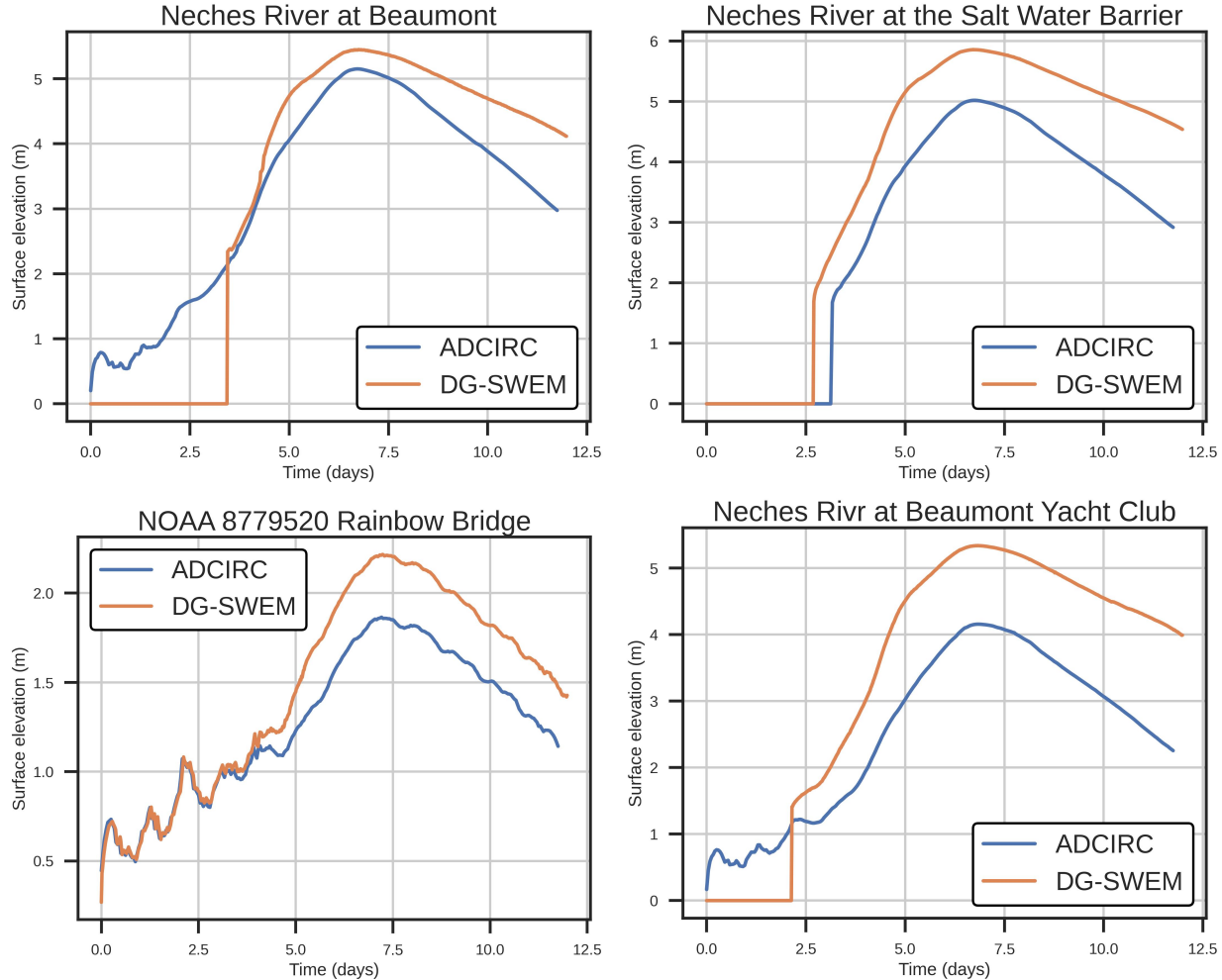


Figure 14: Simulated water elevation from ADCIRC and DG-SWEM at various stations along the Neches River. Flat portions with zero elevation indicate dry nodes. Time is counted from the start of the simulation, and the datum is NAVD88.

In Figure 14, we observe underprediction from ADCIRC in all cases. As ADCIRC relies on the Generalized Wave Continuity Equation (GWCE) — a surrogate to the SWE — we do expect differences in the simulated water surface elevation, particularly in regions of strongly convective flow. The mismatch between wet/dry elevation values at the beginning can be attributed to differences in wetting-and-drying algorithms in the two programs.

4. Concluding Remarks

In this paper, we have presented recent developments to compound flood modeling using DG methods. In particular, we exploit the conservation properties of DG methods to add rainfall as a source to the continuity equation in the shallow water equations. To ascertain spatially and temporally varying rainfall intensity we use parametric rainfall models from literature as well as interpolated rain data from past events.

We have shown results from extensive numerical experiments which highlight the capabilities and properties of our methodology, including conservation properties and compound

flooding during hurricanes with rainfall. In particular, we note the enhancements due to the addition of rainfall in the results for Hurricane Harvey (2017) in the areas close to the hurricane track, indicating the potential of using such parametric rainfall models in compound flood simulations. Comparisons to results from ADCIRC for river runoff in the Neches river further highlights the capabilities of our DG methodology and the solution of the SWE.

While the DG methodology leads to accurate solutions, the increased number of degrees of freedom in the finite element approximation leads to significantly increased run-times when compared to e.g., ADCIRC. To alleviate these costs and make DG-SWEM more viable, we are currently incorporating GPU parallelization as they have been shown to work well with the localized nature of the DG method [36, 37]. Future research directions of interest includes the combination of the DG method with Bubnov-Galerkin, e.g., [38] for increased efficiency as well as splitting methods for implicit-explicit time stepping. In [24], the authors also propose potential enhancements to the R-CLIPER model that will be investigated in future works to increase the fidelity of the simulations.

Acknowledgements

This work has been supported by the United States National Science Foundation NSF PREEVENTS Track 2 Program, under NSF Grant No. 1855047. The authors also would like to gratefully acknowledge the use of the "ADCIRC", "DMS23001", and "DMS21031" allocations on the Frontera supercomputer at the Texas Advanced Computing Center at the University of Texas at Austin.

References

- [1] T. Wahl, S. Jain, J. Bender, S. D. Meyers, M. E. Luther, Increasing risk of compound flooding from storm surge and rainfall for major US cities, *Nature Climate Change* 5 (12) (2015) 1093–1097.
- [2] M. Loveland, A. Kiaghadi, C. N. Dawson, H. S. Rifai, S. Misra, H. Mosser, A. Parola, Developing a modeling framework to simulate compound flooding: When storm surge interacts with riverine flow, *Frontiers in Climate* 2 (2021) 609610.
- [3] F. L. Santiago-Collazo, M. V. Bilskie, S. C. Hagen, A comprehensive review of compound inundation models in low-gradient coastal watersheds, *Environmental Modelling & Software* 119 (2019) 166–181.
- [4] P. Orton, F. Conticello, F. Cioffi, T. Hall, N. Georgas, U. Lall, A. Blumberg, K. MacManus, Flood hazard assessment from storm tides, rain and sea level rise for a tidal river estuary, *Natural hazards* 102 (2) (2020) 729–757.
- [5] K. Kumbier, R. C. Carvalho, A. T. Vafeidis, C. D. Woodroffe, Investigating compound flooding in an estuary using hydrodynamic modelling: a case study from the shoalhaven river, Australia, *Natural Hazards and Earth System Sciences* 18 (2) (2018) 463–477.

- [6] W. J. Pringle, D. Wirasaet, K. J. Roberts, J. J. Westerink, [Global storm tide modeling with adcirc v55: Unstructured mesh design and performance](#), Geoscientific Model Development Discussions 2020 (2020) 1–30. [doi:10.5194/gmd-2020-123](#).
URL <https://gmd.copernicus.org/preprints/gmd-2020-123/>
- [7] R. A. Luettich, J. J. Westerink, N. W. Scheffner, et al., ADCIRC: an advanced three-dimensional circulation model for shelves, coasts, and estuaries. Report 1, theory and methodology of ADCIRC-2DD1 and ADCIRC-3DL (1992).
- [8] C. P. Jelesnianski, SLOSH: Sea, lake, and overland surges from hurricanes, Vol. 48, US Department of Commerce, National Oceanic and Atmospheric Administration, 1992.
- [9] J. Veeramony, A. Condon, M. van Ormondt, Forecasting storm surge and inundation: model validation, Weather and Forecasting 32 (6) (2017) 2045–2063.
- [10] G. Brunner, CEIWR-HEC HEC-RAS river analysis system: User's manual version 6.0, US Army Corps of Engineers Institute for Water Resources, HEC, January: Davis, CA, USA (2021).
- [11] G. W. Brunner, HEC-RAS river analysis system. hydraulic reference manual. version 1.0., Tech. rep., Hydrologic Engineering Center Davis CA (1995).
- [12] C. W. Downer, F. L. Ogden, GSSHA: Model to simulate diverse stream flow producing processes, Journal of Hydrologic Engineering 9 (3) (2004) 161–174.
- [13] S. Takase, K. Kashiyama, S. Tanaka, T. E. Tezduyar, Space–time SUPG formulation of the shallow-water equations, International Journal for Numerical Methods in Fluids 64 (10-12) (2010) 1379–1394.
- [14] E. J. Kubatko, J. J. Westerink, C. Dawson, hp discontinuous Galerkin methods for advection dominated problems in shallow water flow, Computer Methods in Applied Mechanics and Engineering 196 (1-3) (2006) 437–451.
- [15] C. Dawson, E. J. Kubatko, J. J. Westerink, C. Trahan, C. Mirabito, C. Michoski, N. Panda, Discontinuous Galerkin methods for modeling hurricane storm surge, Advances in Water Resources 34 (9) (2011) 1165–1176.
- [16] B. Cockburn, C.-W. Shu, The Runge–Kutta discontinuous Galerkin method for conservation laws v: multidimensional systems, Journal of computational physics 141 (2) (1998) 199–224.
- [17] N. C. for Atmospheric Research (NCAR), Precipitation data sets: Overview & comparison table, <https://climatedataguide.ucar.edu/climate-data/precipitation-data-sets-overview-comparison-table>, accessed: 2023-06-19.
- [18] W. Tan, Shallow water hydrodynamics: Mathematical theory and numerical solution for a two-dimensional system of shallow-water equations, Elsevier, 1992.

- [19] E. J. Kubatko, B. A. Yeager, D. I. Ketcheson, Optimal Strong-Stability-Preserving Runge–Kutta time discretizations for discontinuous galerkin methods, *J. Sci. Comput.* 60 (2) (2014) 313–344.
- [20] C.-W. Shu, TVB uniformly high-order schemes for conservation laws, *Math. Comput.* 49 (179) (1987) 105–121.
- [21] C.-W. Shu, S. Osher, Efficient implementation of essentially non-oscillatory shock-capturing schemes, *J. Comput. Phys.* 77 (2) (1988) 439–471.
- [22] S. Bunya, E. J. Kubatko, J. J. Westerink, C. Dawson, A wetting and drying treatment for the Runge–Kutta discontinuous Galerkin solution to the shallow water equations, *Computer Methods in Applied Mechanics and Engineering* 198 (17-20) (2009) 1548–1562.
- [23] G. J. Holland, An analytic model of the wind and pressure profiles in hurricanes (1980).
- [24] R. E. Tuleya, M. DeMaria, R. J. Kuligowski, Evaluation of GFDL and simple statistical model rainfall forecasts for U.S. landfalling tropical storms, *Weather and Forecasting* 22 (1) (2007) 56–70.
- [25] R. J. LeVeque, Balancing source terms and flux gradients in high-resolution godunov methods: the quasi-steady wave-propagation algorithm, *Journal of computational physics* 146 (1) (1998) 346–365.
- [26] Y. Iwagaki, Fundamental studies of runoff analysis by characteristics, *Bulletin 10, Disaster Prevention Research Institute, Kyoto University, Kyoto, Japan*, 25pp (1955).
- [27] K. Feng, F. J. Molz, A 2-D diffusion-based, wetland flow model, *Journal of Hydrology* 196 (1–4) (1997) 230–250.
- [28] M. Santillana, C. Dawson, A numerical approach to study the properties of solutions of the diffusive wave approximation of the shallow water equations, *Computational Geosciences* 14 (1) (2010) 31–53.
- [29] W. Zhang, T. W. Cundy, Modeling of two-dimensional overland flow, *Water Resources Research* 25 (9) (1989) 2019–2035.
- [30] A. Valle-Levinson, M. Olabarrieta, L. Heilman, Compound flooding in Houston-Galveston bay during hurricane Harvey, *Science of the Total Environment* 747 (2020) 141272.
- [31] E. Blake, D. Zelinsky, Hurricane Harvey. national hurricane center tropical cyclone rep. al092017 (2018).
- [32] J. A. Goff, J. M. Swartz, S. P. Gulick, C. N. Dawson, A. R. de Alegria-Arzaburu, An outflow event on the left side of Hurricane Harvey: Erosion of barrier sand and seaward transport through Aransas Pass, Texas, *Geomorphology* 334 (2019) 44–57.

- [33] C. W. Landsea, J. L. Franklin, Atlantic hurricane database uncertainty and presentation of a new database format, *Monthly Weather Review* 141 (10) (2013) 3576–3592.
- [34] Iowa State University Department of Geological and Atmospheric Sciences, accessed: August 2022. [\[link\]](#).
URL <https://mtarchive.geol.iastate.edu/>
- [35] US Geological Survey, [Flood event viewer](#), accessed: June 2022.
URL <https://stn.wim.usgs.gov/FEV/#2017Harvey>
- [36] A. Klöckner, T. Warburton, J. Bridge, J. S. Hesthaven, Nodal discontinuous galerkin methods on graphics processors, *J. Comput. Phys.* 228 (21) (2009) 7863–7882.
- [37] M. Fuhr, An implementation of the discontinuous galerkin method on graphics processing units, Ph.D. thesis, University of Waterloo (2013).
- [38] C. Dawson, J. Proft, Discontinuous and coupled continuous/discontinuous Galerkin methods for the shallow water equations, *Computer Methods in Applied Mechanics and Engineering* 191 (41-42) (2002) 4721–4746.